Sediment size on talus slopes correlates with fracture spacing on bedrock cliffs: Implications for predicting initial sediment size distributions on hillslopes

5   Joseph P. Verdian[1], Leonard S. Sklar[1,2], Clifford S. Riebe[3], Jeffrey R. Moore[4]

[1]Department of Earth and Climate Sciences, San Francisco State University, San Francisco, 94302, USA
[2]Department of Geography, Planning and Environment, Concordia University, Montreal, H3G1M8, Canada
[3]Department of Geology and Geophysics, University of Wyoming, Laramie, 82071, USA
[3]Department of Geology and Geophysics, University of Utah, Salt Lake City, 84112, USA

Correspondence to: Leonard S. Sklar (leonard.sklar@concordia.ca)

Abstract. The detachment of rock fragments from fractured bedrock on hillslopes creates sediment with an initial size distribution that sets the upper limits on particle size for all subsequent stages in the life of sediment in landscapes. We hypothesize that the initial size distribution should depend on the size distribution of latent sediment (i.e., blocks defined by
15   through-going fractures) and weathering of sediment before or during detachment (e.g., disintegration along crystal grain boundaries). However, the initial size distribution is difficult to measure, because the interface across which sediment is produced is often shielded from view by overlying soil. Here we overcome this limitation by comparing fracture spacings measured from exposed bedrock on cliff faces with particle size distributions in adjacent talus deposits at 15 talus-cliff pairs spanning a wide range of climates and lithologies in California. Median fracture spacing and particle size vary by more than
20   tenfold and correlate strongly with lithology. Fracture spacing and talus size distributions are also closely correlated in central tendency, spread, and shape, with b-axis diameters showing the closest correspondence with fracture spacing at most sites. This suggests that weathering has not modified latent sediment either before or during detachment from the cliff face. In addition, talus has not undergone much weathering after deposition and is slightly coarser than the latent sizes, suggesting that it contains some fractures inherited from bedrock. We introduce a new conceptual framework for understanding the
25   relative importance of latent size and weathering in setting initial sediment size distributions in mountain landscapes. In this framework, hillslopes exist on a spectrum defined by the ratio of two characteristic timescales: the residence time in saprolite and weathered bedrock, and the time required to detach a particle of a characteristic size. At one end of the spectrum, where weathering residence times are negligible, the latent size distribution can be used to predict the initial size distribution. At the other end of the spectrum, where weathering residence times are long, the latent size distribution can be erased by
30   weathering in the critical zone.

1 Introduction

The detachment of rock fragments from fractured or weathered bedrock creates sediment of various sizes that evolve during transport and storage on slopes and in rivers due to chemical and physical weathering. At all stages in the life of sediment, its size distribution influences chemical, physical, and biological processes, including throughflow of reactive fluids in soil

35 (Maher, 2010; Brantley et al., 2011), river incision into bedrock (Sklar and Dietrich, 2004; Turowski et al., 2015), and the reproductive potential of aquatic habitat (Riebe et al., 2014; Overstreet et al., 2015). The first stage begins when particles are detached from saprolite (in soil-mantled landscapes) or fractured bedrock (when soil is absent). The resulting initial size distribution is the starting point for the evolution of the size distribution on the hillslope where the sediment is produced and therefore sets the upper limits on particle size distributions at each successive stage in the sediment's life (Sklar et al., 2017;

40 Roda-Boluda et al., 2018). Particle shape also evolves during transport downstream and can be used to estimate the distance traveled from the particle's source when initial shape is known (Miller et al., 2014; Szabo et al., 2015). However, the factors that regulate variability in particle shape and the initial sediment size distribution are poorly understood.

The initial size distribution and initial particle shape should depend both on the size distribution of latent blocks in bedrock

45 and on the characteristic length scales of subsequent weathering processes. The "latent" size distribution is set by the spacing and orientation of fractures, foliations, bedding planes, and mineral grain boundaries. These represent preexisting planes of weakness and determine the volume and shape of newly created sediment particles, which can be quantified by measuring the distributions of the major-, intermediate-, and minor-axis particle diameters. The three-dimensional template for latent particles should depend on conditions experienced during formation of the rock at depth, including rate of cooling for

50 igneous rocks (Lore et al., 2001), pressure and temperature for metamorphic rocks (Manda et al., 2008), and deposition and diagenesis in sedimentary rocks (Narr and Suppe, 1991). These factors are overprinted by fracturing induced by the evolving stress field experienced by the rock as it is exhumed from deep in the crust (Molnar et al., 2007; Leith et al., 2014; Moon et al., 2017). Thus the latent size distribution reflects everything that has happened to the rock before experiencing weathering in the near-surface environment. As weathering commences, but before particles are detached, physical and chemical

55 processes can create new surfaces that can be exploited during detachment. Hence, the initial size distribution should also depend on the characteristic length scales of weathering processes, such as mineral expansion, segregation ice growth, root wedging, and animal burrowing, particularly on slopes where preexisting planes of weakness in bedrock are widely spaced (Sklar et al., 2017; Messenzehl et al., 2018). In addition to these physical weathering processes, chemical reactions such as mineral dissolution can create new planes of weakness and thus influence the initial size distribution created during

60 detachment (Fletcher and Brantley, 2010; Brantley et al., 2011; Goodfellow et al., 2016). Although these hypotheses are both intuitive and mechanistic, to our knowledge, the relative importance of latent sizes and weathering in initial size distributions has not been systematically explored. The initial detachment of rock fragments is generally hidden from view under soil, saprolite, and weathered rock, and sizes can therefore evolve before they can be accessed and measured. This makes it difficult to isolate the influence of the latent size distribution from the effects of weathering processes.

65

To overcome this limitation, previous studies have compared fracture spacings measured from exposed bedrock on cliff faces with particle size distributions in adjacent sediment deposits. For example, at Inyo Creek, on the east side of the Sierra Nevada, California, where hillslope sediment size distributions are bimodal, in-situ measurements from bedrock cliff faces show that fracture spacing distributions do not vary with elevation and closely correspond with the likewise spatially

70 invariant coarse mode of the hillslope particle size distribution (Sklar et al., 2020). Elsewhere in California, at two sites with differing fracture spacing distributions, particle sizes in stream sediment correlate with fracture spacings measured in adjacent bedrock cliff faces at locations where the sediment contributing area is dominated by bare bedrock (Neely and DiBiasi, 2020). Results from both of these studies are consistent with latent sizes in bedrock dominating over weathering on slopes in regulating the initial size distribution of coarse sediment. In contrast, results from a suite of sites in the Swiss Alps

75 suggest that weathering by frost cracking can impose a characteristic scale upon talus particle sizes, leading to poor correlations with fracture spacing distributions on adjacent bedrock cliffs (Messenzehl et al., 2018).

Here we quantify correlations between initial sediment size and fracture spacing distributions across 15 talus-cliff pairs spanning a wide range of settings, including rock types and climatic conditions not investigated in previous work. Our sites

80 span a 3000-m range in elevation across granodiorite, andesite, basalt, metasedimentary, and chert lithologies in California. Thus our study design allows us to test the null hypothesis that the initial sizes closely match latent sizes across a wide, geologically driven range in latent size distributions. An alternate hypothesis is that talus cones and the latent size distribution exposed in cliff faces are not strongly correlated for one or both of the following reasons: (i) blocks are detached along only a subset of preexisting fractures, for example because of unequal fracture persistence (Kim et al., 2007), or along

85 newly formed fractures, as in the case of grus production from granite with low fracture density (Wahrhaftig, 1965); (ii) physical or chemical weathering reduces particle sizes after the talus is detached from the cliff, for example when particles hit the adjacent slope or as they sit in the talus deposit. Neither of these alternatives to the null hypothesis are consistent with our results. Measurements of central tendency, spread, and shape of the talus size and fracture spacing distributions all correlate strongly across a 40-fold variation in median fracture spacing. We also found statistically significant differences in

90 mean talus shape among rock types, contrary to the null hypothesis that initial particle shape is invariant for blocks produced from bedrock by mechanical weathering (Domokos et al., 2015). Together these results confirm that initial sediment size distributions can be predicted from fracture spacing distributions at sites where the latent size distribution dominates over weathering. They also imply that lithologic and tectonic controls on latent size distributions can have a strong influence on the initial size and shape of individual particles and thus on the evolution of particle size distributions across landscapes. To

95 generalize our findings beyond the talus-cliff pairs studied here, we introduce a conceptual framework for quantifying the relative importance of latent sizes and weathering using the timescale of detachment of latent particles and the timescale of weathering that occurs before the particle is detached.

2 Methods

100 To test the null hypothesis about strong connections between latent size and initial size and shape of sediment, we selected 15 cliff faces and adjacent talus slopes at five sites in California, USA (Fig. 1). The talus-cliff pairs in the Sierra Nevada represent a subset of bedrock slopes featured in previous work on connections between rock-mass strength and cliff retreat rates (Moore et al., 2009). These include ten slopes in the vicinity of Conness Basin, Mount Tallac, and Ebbetts Pass (Table 1), three sites where differences in lithology correspond to differences in average fracture spacing. To diversify the range of conditions that might contribute to differences in weathering and thereby produce deviations from the null hypothesis, we

105 selected a series of five additional talus-cliff pairs at Grizzly Peak and Twin Peaks, two sites in the San Francisco Bay Area (Table 1).

2.1 Fracture spacing distributions on cliff faces

To quantify fracture spacing at each site, we used a horizontal scan line (Moore et al., 2009) consisting of a survey tape stretched across the cliff face at a constant elevation (e.g., Fig. 2). The height of the scan line above the top of the adjacent

110 talus cone ranged from 0.3 to 1.5 meters in our study, depending mostly on ease of sampling. Our approach assumes that fracture spacing along a single horizontal line is representative of the contributing area of the talus, including unreachable sections above the scan line. We set the length of each scan line equal to the width of contact between the cliff face and its adjacent talus cone, which ranged between 5- and 15-meters long across our sites. Thus we limited our measurements of fracture spacing to the width of the talus source area. Along each scan line, we measured the position of every fracture that

115 crossed the tape, irrespective of orientation. This yields a distribution of fracture spacings measured as the distance between successive fractures. Our goal was to sample the spacing between fractures that could produce a particle via rockfall. Thus we focused on open, through-going fractures with spacings greater than 2 mm, ignoring changes in surface roughness and other rock defects that did not extend far enough to intersect other fractures on the cliff face. This ignores the potential role of microfracturing at the scale of mineral grains (Eppes and Keanini, 2017) in generating detachable particles on the cliff

120 faces.

2.2 Particle size distributions in talus cones

To quantify surface particle size distributions in talus at each of the Sierra Nevada talus-cliff pairs, we measured the a-, b-, and c-axis diameters of particles at evenly-spaced points along three slope-parallel transects extending from the base of the cliff to the toe of the talus slope (e.g., Fig. 2). To measure sizes of an equal number of particles on each slope, we divided the

125 sum of the three tape lengths by 100, and used the result to define the sample spacing, which varied from 2.5 to 1 m across the sites. At each sampling point, we used a ruler to measure sizes of particles with diameters less than 300 mm and stadia rods to measure sizes for everything else. We matched the precision of the fracture spacing measurements by rounding particle diameters to the nearest millimeter and lumping diameters less than 2 mm into a <2 mm bin. In some cases, the a-, b-,

and/or c-axis could not be readily measured because the particle was too heavy to move and thus to fully expose it for

130   identification of long, intermediate, and short axis orientations. In those cases, we assumed that the c axis was perpendicular to the surface slope and estimated the a- and b-axis diameters using the two longest exposed axes. We then estimated a minimum value for the c axis as the height of the particle normal to the slope.

The even spacing in our talus sampling approach should yield a representative particle size distribution, even if size-selective

135   transport leads to downslope coarsening, which is commonly observed on angle-of-repose slopes (Kirkby and Stratham, 1975). This coarsening arises because finer particles have larger friction angles and therefore travel shorter distances before coming to rest in the talus cone. Because size-selective disentrainment occurs across the entire slope, the talus surface can be treated as a single population whose grain size distribution can be quantified representatively by uniformly spaced sampling.

140   We addressed the potential for bias due to kinetic sieving (a vertical sorting process) by supplementing our surface-based measurements with bulk samples of relatively fine subsurface sediment accessed through openings between particles at the surface at five of the Sierra Nevada talus-cliff pairs. The particle size distribution of each ~2 kg sample was measured in the lab by standard mechanical sieving. These subsurface size distributions should match the fine tail of the latent size distribution measured in the scan lines if the null hypothesis is correct (i.e., the initial size distribution is strongly controlled

145   by the latent size distribution).

At the two San Francisco Bay Area sites, where the talus cones are relatively small, we measured surface particle size distributions using standard random point counting methods (Bunte and Abt, 2001) to sample 100 particles from each talus cone. At the Grizzly Peak site, we used rulers to quantify a-, b-, and c-axis diameters of sampled particles. At the Twin Peaks

150   site, where talus produced from both pillow basalt and ribbon chert were small compared to talus produced at the other sites, we used a mix of calipers and rulers to quantify just the b-axis diameters.

3 Results and Interpretations

Spacings between individual fractures on cliff faces range from 2 to 5000 mm across the suite of sites, with median spacings at individual sites ranging from 10 to 390 mm (Table 2). Particle sizes span a similar range, with a-axis diameters as large as

155   5450 mm, c-axis diameters as small as 2 mm, and median b-axis diameters ranging from 10 to 575 mm. Both fracture spacing and particle size vary systematically with lithology: Granodiorite sites have the largest fracture spacings and particle sizes while the pillow basalt site has the smallest (Fig. 3).

At each site, the distribution of particle sizes in talus closely corresponds to the distribution of fracture spacings on adjacent

160   cliffs. This is evident in both the similar shape and overlap of the size and spacing distributions (Fig. 3). For example, at most of the sites, the cumulative empirical distribution function (EDF) of fracture spacing is parallel to the EDFs of particle

size, which are also generally parallel to each other where the a-, b-, and c-axis diameters were measured together (Fig. 3). In many cases, the EDFs of size and spacing also overlap for at least one of the particle diameters. For example, at CB-1, the fracture spacing distribution closely overlaps with the size distribution of the a-axis particle diameters (Fig. 3e). In contrast, the overlap is closest with the b-axis diameters at EP-26, TP-1, and TP-3, and with the c-axis diameters at both MT-38 and CB-5. Only two of the sites (CB-2 and CB-3) have particle diameter EDFs that do not closely parallel the fracture spacing EDF, and only one (MT-39) has a fracture spacing EDF that plots outside the envelope defined by the a- and c-axis diameters.

The close correspondence between distributions at each talus-cliff pair is reflected in cross-site correlations between the central tendency of fracture spacing and particle size distributions for each of the three particle axes (Fig. 4). In each case, the increase in median particle diameter with increasing fracture spacing follows a trend with a slope that is statistically indistinguishable ($p>0.45$) from a 1:1 relationship in log-log space (Fig. 4a–c). This suggests that the correspondence is scale-independent—and also independent of rock type—across the full range of measured sizes (up to two orders of magnitude for the b-axis diameters). The vertical offset between the trend and the 1:1 line is smallest for the b-axis diameters (Fig. 4b), which are 42% larger on average than the fracture spacing. The c-axis diameters have a slightly larger offset, plotting below the 1:1 line (Fig. 4c), while the a-axis diameters have the largest offset, with median diameters that are systematically greater than the median fracture spacing by a factor of ~2.5 (Fig. 4a). Given that the b-axis is the characteristic dimension that scales most closely with volume, the close correspondence between the b-axis diameters and fracture spacings (Fig. 4b) is consistent with talus production from cliffs by spallation of blocks defined by intersecting fractures without substantial size reduction during deposition.

The connection between talus particles and blocks exposed on cliff faces is further supported by the close correspondence between the spread in the b-axis diameter and fracture spacing distributions (Fig. 4d). The relationship between the geometric standard deviation of the b-axis diameters and fracture spacing across all sites is statistically indistinguishable from a 1:1 relationship ($p>0.67$), reflecting the parallel EDFs of the b-axis diameters and fracture spacings evident at many of the sites in Fig. 3. Thus, both the central tendency and spread in the size and spacing distributions are closely coupled across the range of rock types and climates spanned by our study sites.

A third aspect of the particle size and fracture spacing distributions that we explored is distribution shape. To determine if there was a match in shape between the distributions, we first fit exponential, log-normal, and power distributions to the data, recognizing that fracture spacing distributions in rock commonly have shapes that follow one of these distributions (Gillespie et al., 1993). For both the fracture spacing and talus size distributions, we found that the Weibull form of the exponential distribution yielded the best fit to the data in most cases. The degree to which the data follow a Weibull distribution at each site is illustrated in Figure 5. Data that plot on a straight line in the Weibull probability space defined by the plot axes are

indicative of a population sampled from a Weibull distribution. In addition, because the particle size and fracture spacing measurements are normalized to their respective medians, cumulative distributions that coincide in the plotting space are indicative of population distributions that have the same shape. For most sites, both the particle size and fracture spacing data fall along straight lines and often closely coincide, as in the case of MT-38, CB-1, CB-5, and TP-1, indicating that they

200 share roughly the same Weibull distributions. In some cases, the slope of the b-axis distribution is steeper than the fracture spacing distribution, as in the case of MT-39 and CB-3, indicative of narrower particle size distributions and consistent with the systematically lower geometric standard deviations at these sites (Fig. 4d). In some cases, the lower tails of the distributions follow a steeper trend than the rest of the data, as in the case of CB-3, GP-1, and EP-26, potentially reflecting an undersampling of the smallest fractures that could result from the limited sample size and our emphasis on quantifying

205 spacings of throughgoing fractures in the scan lines. The one rock type with data that deviate substantially from the Weibull distribution is the chert: at TP-3 and especially at TP-4, the data show curvature in the Weibull space, and the particle size and fracture spacing distributions do not closely match. Aside from these exceptions, the fracture spacing and talus size distributions have similar shapes (Figs. 3 and 5) and are closely correlated in their central tendencies and spreads across all six lithologies (Fig. 4), consistent with our hypothesis that fracture spacing distributions can be used to predict initial particle

210 size distributions in sediment.

Our talus size measurements do not, in contrast, support the null hypothesis that initial particle shape is invariant for blocks produced by mechanical weathering. We quantified shape at the 11 sites where we measured the a-, b-, and c-axes diameters by calculating b:a and c:a ratios, which can be plotted together on a ternary diagram that displays rods, slabs, and equisided

215 blocks at the vertices (Fig. 6, after Sneed and Folk, 1958). At many of the sites, individual particles span nearly the full range of shapes represented in the diagram. Within each rock type there is little site-to-site variability in mean particle shape, suggesting that we can group sites together by rock type. When we do, we find statistically significant differences in mean particle shape among some rock types, despite substantial overlap in the distributions of individual shapes among the lithologies (Fig. 6). For example, talus produced from the metasediment has lower mean b:a and c:a ratios and therefore is

220 more elongate on average than talus produced from the granodiorite (Fig. 6a). In addition, andesite particles are more slab-like than basalt on average, with a lower mean c:a ratio (Fig. 6b). In both of these comparisons, many of the talus deposits have similar elevation and therefore similar climatic conditions (Table 1), indicating that the differences in shape among the rock types are due to intrinsic differences in bedrock rather than differences in weathering environment. Of the six possible comparisons, only one—between the granodiorite and basalt—had no statistically significant differences in either axis ratio.

225 In the three remaining comparisons, metasediment has a lower mean b:a ratio than andesite; metasediment also has a lower mean b:a and a:c than the basalt; and finally the andesite has a lower mean c:a ratio than the granodiorite. Given the overlap in mean shape between the granodiorite and the basalt, which differ in mean particle size by up to a factor of 10 (Fig. 4), there is no evidence in our data that initial particle shape varies with size, contrary to the prediction from previous work that smaller particles should be more block-like on average (Domokos et al., 2015). Our results show that different rock types

230 have different initial b:a ratios and thus conflict with the prediction that the b:a ratio should have a single average value for particles produced by mechanical weathering. This suggests that lithology-specific values for initial shape may be needed when using shape to infer distance traveled from sediment sources (Miller et al., 2014; Szabo et al., 2015; Novak-Szabo et al., 2018), particularly for lithologies that have foliation and other anisotropic properties.

4 Discussion

235 The close correlation between talus size and fracture spacing distributions at our sites (Figs. 3–5) suggests that particles are detached from nearly the full network of fractures exposed on the cliff faces and do not undergo much size reduction due to physical or chemical weathering in talus deposits. This finding, while limited to our sites, is robust across a wide range of lithologies and weathering conditions, suggesting that it spans a range of processes that could lead to particle detachment and subsequent weathering in talus deposits, including subcritical cracking and segregation ice growth.

240

Of the three particle dimensions measured here, the distribution of b-axis diameters most closely matches the fracture spacing distributions (Figs. 3–5). This suggests that fracture spacing measurements can be used to predict the initial size distribution of intermediate particle diameters. This is useful because the b-axis diameter is the most characteristic linear measure of particle volume and is therefore commonly used to represent particle mass in sediment transport theory and

245 applications (Bagnold, 1966). Nevertheless, across our sites the b-axis is systematically ~½ phi interval larger on average than the median fracture spacing (Fig 4b); only two in 15 sites have a median b-axis diameter less than the median fracture spacing, which is unlikely to arise by chance ($p = 0.0064$). The positive deviations shown in Figure 4 contrast with previous measurements from other mountain landscapes in California, where sediment sizes also correlate strongly with—but are systematically finer than—fracture spacings in the source bedrock (Neely and DiBiasi, 2020; Sklar et al., 2020). At our sites,

250 the systematically coarser b-axis diameters may be driven, in part, by vertical sorting that causes fine particles to be underrepresented in point counts conducted on talus slope surfaces. However, we find no evidence of this in our measurements of sediment extracted from openings between surface particles: at each site where we made these measurements, the size distributions of the bulk samples overlap sufficiently the fine tail of the talus distribution that they can be combined using established techniques (Bunte and Abt, 2001) into a single continuous distribution in which the

255 median is equal to the median of the distribution of talus at the surface. This suggests that analysis of the talus at the surface provides unbiased estimates of the size distributions of material shed from cliff faces at our sites. Hence, we interpret the positive offset in b-axis diameters (Fig. 4b) to reflect incomplete use of exposed fractures during detachment of talus from cliff faces. These unused fractures are presumably contained within the talus blocks in the deposit and may be exploited during later size reduction by physical and chemical weathering.

260

Our analysis suggests that there are no systematic site-to-site deviations from the 1:1 trend between median b-axis diameters and median fracture spacings, despite the large differences in climate and thus weathering environment (Table 1). Moreover, there is no significant trend in residuals relative to the 1:1 trend with either mean annual temperature or average annual precipitation. This implies that the latent size distribution (embedded within the fractures exposed on the cliff faces)

265 dominates over weathering as the main control on the particle sizes produced on slopes across our sites.

The dominance of latent size over weathering is also supported by previous analyses of correlations between fracture density and erosion rates at the Sierra Nevada sites, where talus deposit volumes accumulated since deglaciation ~13,000 years ago were used to quantify cliff retreat rates (Moore et al., 2009). Higher fracture density (and thus lower fracture spacing)

270 corresponds to faster cliff retreat rates (Table 2), because denser fractures contribute to lower rock mass strength, and thus make bedrock cliffs more susceptible to erosion (Howard and Selby, 2009; Moore et al., 2009). Thus, at these sites, where weathering is minimal and cliffs are still responding to deglaciation, fracture spacing controls both initial size and the production rate of sediment through its effects on rock mass strength. In soil mantled landscapes, in contrast, where hillslope erosion rates are set by stream incision rates, theory and observations suggest that faster erosion should generally lead to

275 larger particle sizes due to lower regolith residence times (T_R) and thus less-extensive weathering in the critical zone (Sklar et al., 2017; Callahan et al., 2019). At our Sierra Nevada sites, and in general at other sites where $T_R \sim 0$, latent size should commonly dominate over weathering in setting initial particle size distributions.

Our analysis of cliff retreat rates and fracture spacings from the Sierra Nevada points to another potentially insightful

280 timescale: T_P (T), the time required to liberate a latent particle having the characteristic, median size, calculated following Eq. (1):

$$T_P = F_{50}/E \tag{1}$$

Here, F_{50} is the median fracture spacing (L), a proxy for the characteristic latent particle size, and E is the erosion rate of the fractured bedrock surface (L/T), equal to the cliff retreat rate at the Sierra Nevada sites. Application of Equation 1 to data

285 from our sites indicates that T_P ranges from as short as 88 years to produce a layer of 60-mm diameter latent particles at EP-26, the most rapidly eroding cliff face, to as long as 16,500 years to produce 330-mm diameter particles at CB-1, indicating that the entire post-glacial accumulation time and more was needed to detach a single layer of latent particles with the characteristic median size at the most slowly eroding cliff face (Table 2). The calculated T_P at the remaining talus-cliff pairs in the Sierra Nevada sites is less than 13,000 years, consistent with the assumption in the erosion rate calculations (Moore et

290 al., 2009) that all of the sediment was produced after the glaciers retreated.

The relative importance of latent size and weathering can be evaluated by quantifying the ratio of T_R to T_P, as in Eq. (2):

$$T_R/T_P = \frac{H}{E}\bigg/\frac{F_{50}}{E} = H/F_{50} \tag{2}$$

Here, H is the thickness of saprolite and weathered rock (L), and the erosion rate at the top of fractured rock is assumed to be equal to the erosion rate at the base of soil (such that the thickness of saprolite and weathered rock is in steady state). At our sites, which represent an extreme end member with no saprolite or weathered bedrock (i.e., $H{\sim}0$), $T_R/T_P \ll 1$, and the latent size distribution dominates over weathering in setting initial particle size. In contrast, weathering may dominate over latent size distributions when $T_R/T_P \gg 1$, at the other endmember, where erosion is slow, saprolite and/or weathered bedrock is thick, and fractures are closely spaced. In between the two endmembers, we envision a spectrum in the relative importance of weathering and latent size as a function of T_R/T_P. This spectrum is illustrated conceptually in Figure 7 for three cases with the same slope and erosion rate: Increasing saprolite and weathered bedrock thickness and decreasing fracture spacing should lead to higher T_R/T_P ratios (from left to right in Fig. 7), which in turn would correspond to finer initial sediment size distributions produced at the top of fractured bedrock or saprolite (cf. Fig. 7a, b, and c). Fig. 7a depicts a case at the transition from bare bedrock (e.g., the cliff faces studied here), to slopes with patchy soil cover, such as those observed at the other California sites where fracture spacing and sediment size have been quantified (Neely and DiBiasi, 2020; Sklar et al., 2020). Such sites should have enhanced potential for weathering relative to our sites. This might help explain why the median b-axis diameters plot higher than median fracture spacings at our sites and vice versa at the other sites in California. In landscapes that are completely covered with regolith and weathered rock (Fig. 7b–c), the signal of the latent size distribution (and also of initial shape; Fig. 6) may fade before liberation of sediment into the soil. Thus, initial size should be dominated by weathering as residence times increase and thereby increase in exposure to chemical and physical weathering (Fig. 7c).

5 Conclusions

The detachment of rock fragments from fractured bedrock on hillslopes creates sediment with initial size distributions that set the upper limits on particle size for all subsequent stages in the life of sediment as it is exposed to chemical and physical weathering during transport from source to sink. We hypothesize that the initial size distribution should depend on two main factors: the size distribution of latent sediment (i.e., blocks defined by throughgoing fractures); and weathering that occurs in fractured bedrock both before the sediment is detached and during the detachment process (e.g., disintegration along crystal grain boundaries). However, the initial size distribution is difficult to measure, because the interface across which sediment is produced is often shielded from view by overlying soil. Talus deposits that have accumulated beneath cliff faces offer an opportunity to test the hypothesis that, when weathering is minimal, the initial size distribution should strongly reflect the latent size distribution defined by fractures on the cliff faces.

Here, we presented measurements of fracture spacing and particle size distributions from talus-cliff pairs spanning a wide range of climates and lithologies in California. Median fracture spacing varies by a factor of 40, median particle size varies by a factor of 60, and both of these variables correlate strongly with lithology. In addition, fracture spacing and talus size

distributions are closely correlated with each other in central tendency, spread, and shape, with b-axis diameters showing the closest correspondence with the fracture spacing at most sites. This suggests that weathering has not modified latent sediment, either before or during detachment from the cliff face. In addition, talus has not undergone much weathering after deposition and is slightly coarser than the latent sizes implied by the fractures, suggesting that the talus contains unexploited

330   fractures inherited from the cliff face. These results differ from previous work elsewhere in California, where b-axis diameters are systematically finer than bedrock fracture spacings, likely due to post-detachment weathering in the patchy soil deposits where particles were sampled (Neely and DiBiasi, 2020; Sklar et al., 2020). Together, these observations support a new conceptual framework illustrating the relative importance of latent size distributions and weathering on setting the initial sediment size distribution in mountain landscapes. In this framework, hillslopes occupy a spectrum defined by the ratio of

335   two characteristic timescales: the residence time in saprolite and weathered bedrock, and the time required to detach the characteristic particle size. Where weathering residence times are negligible, as at our 15 talus-cliff pairs, the latent size distribution can be used to predict the initial size distribution. At the other end of the spectrum, where weathering residence times are long, the latent size distribution will provide limited predictive information about initial sediment distributions.

Data Availability

340   The data that support the findings of this study will be openly available at
https://dataverse.scholarsportal.info/dataverse/esurf-2020

Author Contributions

JV, LS, and JM designed the field investigation and JV and LS carried it out. JV, LS, and CR analyzed the data. LS and CR prepared the manuscript with contributions from all co-authors.

345   **Competing interests**

The authors declare that they have no conflict of interest

Acknowledgments

The authors thank Nolen Brown, Navek Ceja, Van Jackson-Weaver, Bradley Penner, Paul Vawter, and Dan Rosenburg for assistance in the field; Russell Callahan for assistance with graphic design in Figure 1; and John Caskey and Zan Stine for

350   helpful discussions. Funded by the National Science Foundation grants EAR 1324830 to Sklar and EAR 1325033 to Riebe.

Additional support for Verdian and Sklar provided by the Doris and David Dawdy Fund for Hydrological Science at San Francisco State University.

References

355   Bagnold, R. A.: An approach to the sediment transport problem from general physics, USGS Professional Paper 422-I, US government printing office, Washington DC, 1966.

Brantley, S. L., Buss, H., Lebedeva, M., Fletcher, R. C., and Ma, L.: Investigating the complex interface where bedrock transforms to regolith, Applied Geochemistry, 26, S12-S15, doi:10.1016/j.apgeochem.2011.03.017, 2011.

Bunte, K., and Abt, S. R.: Sampling surface and subsurface particle-size distributions in wadable gravel-and cobble-bed streams for analyses in sediment transport, hydraulics, and streambed monitoring, Gen. Tech. Rep. RMRS-GTR-74. Fort
360   Collins, CO: US Department of Agriculture, Forest Service, Rocky Mountain Research Station. 428 p., 2001.

Callahan, R. P., Ferrier, K. L., Dixon, J., Dosseto, A., Hahm, W. J., Jessup, B. S., Miller, S. N., Hunsaker, C. T., Johnson, D. W., Sklar, L. S., and Riebe, C. S.: Arrested development: Erosional equilibrium in the southern Sierra Nevada, California, maintained by feedbacks between channel incision and hillslope sediment production, GSA Bulletin, 131, 7-8, 1179-1202, doi:10.1130/B35006.1, 2019.

365   Domokos, G., Kun, F., Sipos, A.A. and Szabó, T.: Universality of fragment shapes, Scientific reports, 5, p. 9147, doi:10.1038/srep09147, 2015.

Eppes, M. C., and Keanini, R.: Mechanical weathering and rock erosion by climate-dependent subcritical cracking, Reviews of Geophysics, 55, 2, 470-508, doi:10.1002/2017RG000557, 2017.

Fletcher, R. C., and Brantley, S. L.: Reduction of bedrock blocks as corestones in the weathering profile: observations and
370   model, American Journal of Science, 310, 3, 131-164, doi:10.2475/03.2010.01, 2010.

Gillespie, P. A., Howard, C. B., Walsh, J. J., and Watterson, J.: Measurement and characterisation of spatial distributions of fractures, Tectonophysics, 226, 1-4, 113-141, doi:10.1016/0040-1951(93)90114-Y, 1993.

Goodfellow, B. W., Hilley, G. E., Webb, S. M., Sklar, L. S., Moon, S., and Olson, C. A.: The chemical, mechanical, and hydrological evolution of weathering granitoid, Journal of Geophysical Research: Earth Surface, 121, 8, 1410-1435,
375   doi:10.1002/2016JF003822, 2016.

Graham, D. J. and Midgley, N. G.: Graphical representation of particle shape using triangular diagrams: an Excel spreadsheet method, Earth Surface Processes and Landforms, 25, 13, 1473-1477, doi:10.1002/1096-9837(200012)25:13<1473::AID-ESP158>3.0.CO;2-C, 2000.

Howard, A. D., and Selby, M. J.: Rock slopes, In: Parsons A. J., Abrahams A. D. (eds) Geomorphology of Desert
380   Environments (pp. 189-232), Springer, Dordrecht, doi:10.1007/978-1-4020-5719-9_8, 2009.

Kim, B. H., Cai, M., Kaiser, P. K., and Yang, H. S.: Estimation of block sizes for rock masses with non-persistent joints, Rock Mechanics and Rock Engineering, 40, 2, 169, doi:10.1007/s00603-006-0093-8, 2007.

Kirkby, M. J. and Statham, I.: Surface stone movement and scree formation, The Journal of Geology, 83, 3, 349-362, doi:10.1086/628097, 1975.

385 Leith, K., Moore, J. R., Amann, F., and Loew, S.: In situ stress control on micro-crack generation and macroscopic extensional fracture in exhuming bedrock, Journal of Geophysical Research, 119, 1-22, doi: 10.1002/2012JB009801, 2014.

Lore, J., Aydin, A. and Goodson, K.: A deterministic methodology for prediction of fracture distribution in basaltic multiflows, Journal of Geophysical Research: Solid Earth, 106, B4, 6447-6459, doi:10.1029/2000JB900407, 2001.

390 Maher, K.: The dependence of chemical weathering rates on fluid residence time, Earth and Planetary Science Letters, 294, 1-2, 101-110, doi:10.1016/j.epsl.2010.03.010, 2010.

Manda, A. K., Mabee, S. B., and Wise, D. U.: Influence of rock fabric on fracture attribute distribution and implications for groundwater flow in the Nashoba Terrane, eastern Massachusetts, Journal of Structural Geology, 30, 4, 464-477, doi:10.1016/j.jsg.2007.12.006, 2008.

395 Messenzehl, K., Viles, H., Otto, J. C., Ewald, A., and Dikau, R.: Linking rock weathering, rockwall instability and rockfall supply on talus slopes in glaciated hanging valleys (Swiss Alps), Permafrost and Periglacial Processes, 29, 3, 135-151, doi:10.1002/ppp.1976, 2018.

Miller, K. L., Szabó, T., Jerolmack, D. J., and Domokos, G.: Quantifying the significance of abrasion and selective transport for downstream fluvial grain size evolution, Journal of Geophysical Research: Earth Surface, 119, 11, 2412-2429,
400 doi:10.1002/2014JF003156, 2014.

Molnar, P., Anderson, R. S., and Anderson, S. P.: Tectonics, fracturing of rock, and erosion, Journal of Geophysical Research: Earth Surface, 112, F3, doi:10.1029/2005JF000433, 2007.

Moon, S., Perron, J. T., Martel, S. J., Holbrook, W. S., and St. Clair, J.: A model of three-dimensional topographic stresses with implications for bedrock fractures, surface processes, and landscape evolution, Journal of Geophysical Research:
405 Earth Surface, 122, 4, 823-846, doi:10.1002/2016JF004155, 2017.

Moore, J. R., Sanders, J. W., Dietrich, W. E. and Glaser, S. D.: Influence of rock mass strength on the erosion rate of alpine cliffs, Earth Surface Processes and Landforms, 34, 10, 1339-1352, doi:10.1002/esp.1821, 2009.

Narr, W., and Suppe, J.: Joint spacing in sedimentary rocks, Journal of Structural Geology, 13, 9, 1037-1048, doi:10.1016/0191-8141(91)90055-N, 1991.

410 Neely, A. B. and DiBiase, R. A.: Drainage area, bedrock fracture spacing, and weathering controls on landscape-scale patterns in surface sediment grain size, ESSOAr [preprint], doi:10.1002/essoar.10502617.1, 11 June 2020.

Novak-Szabo, T., Sipos, A. Á., Shaw, S., Bertoni, D., Pozzebon, A., Grottoli, E., Sarti, G., Ciavola, P., Domokos, G. and Jerolmack, D. J.: Universal characteristics of particle shape evolution by bed-load chipping, Science advances, 4,3, doi:10.1126/sciadv.aao4946, 2018.

415 Overstreet, B. T., Riebe, C. S., Wooster, J. K., Sklar, L. S., and Bellugi, D.: Tools for gauging the capacity of salmon spawning substrates, Earth Surface Processes and Landforms, 41, 1, 130-142, doi:10.1002/esp.3831, 2016.

Prism Climate Group, Oregon State University, http://prism.oregonstate.edu, last access: 11 December, 2019.

Riebe, C. S., Sklar, L. S., Overstreet, B. T., and Wooster, J. K.: Optimal reproduction in salmon spawning substrates linked to grain size and fish length, Water Resources Research, 50, 2, 898-918, doi:10.1002/2013WR014231, 2014.

420   Roda-Boluda, D. C., D'Arcy, M., McDonald, J., and Whittaker, A. C.: Lithological controls on hillslope sediment supply: insights from landslide activity and grain size distributions, Earth Surface Processes and Landforms, 43, 5, 956-977, https://doi.org/10.1002/esp.4281, 2018.

Sklar, L. S., and Dietrich, W. E.: A mechanistic model for river incision into bedrock by saltating bed load, Water Resources Research, 40, 6, doi:10.1029/2003WR002496, 2004.

425   Sklar, L. S., Riebe, C. S., Marshall, J. A., Genetti, J., Leclere, S., Lukens, C. L. and Merces, V.: The problem of predicting the size distribution of sediment supplied by hillslopes to rivers, Geomorphology, 277, 31-49, doi:10.1016/j.geomorph.2016.05.005, 2017.

Sklar, L. S., Riebe, C. S., Genetti, J., Leclere, S. and Lukens, C. E.: Downvalley fining of hillslope sediment in an alpine catchment: implications for downstream fining of sediment flux in mountain rivers, Earth Surface Processes and
430   Landforms, 45, 8, 1828-1845, doi:10.1002/esp.4849, 2020.

Sneed, E. D. and Folk, R. L.: Pebbles in the lower Colorado River, Texas a study in particle morphogenesis, The Journal of Geology, 66, 2, 114-150, doi:10.1086/626490, 1958.

Szabó, T., Domokos, G., Grotzinger, J. P., and Jerolmack, D. J.: Reconstructing the transport history of pebbles on Mars, Nature communications, 6, 1, doi:10.1038/ncomms9366, 2015.

435   Turowski, J. M., Wyss, C. R., and Beer, A. R.: Grain size effects on energy delivery to the streambed and links to bedrock erosion, Geophysical Research Letters, 42, 6, 1775-1780, doi:10.1002/2015GL063159, 2015.

Wahrhaftig, C.: Stepped topography of the southern Sierra Nevada, California, Geological Society of America Bulletin, 76, 10, 1165-1190, doi:10.1130/0016-7606(1965)76[1165:STOTSS]2.0.CO;2, 1965.

440

Table 1. Study sites in Sierra Nevada and San Francisco Bay Area

Location	Pair	Lithology	Latitude (°N)	Longitude (°W)	Elevation (m)	MAT[1] (°C)	MAP[2] (mm)
Conness Basin	CB-1	Granodiorite	37.9763	119.3082	3262	1.3	1190
Conness Basin	CB-2	Granodiorite	37.9750	119.3033	3293	1.1	1226
Conness Basin	CB-3	Granodiorite	37.9797	119.3006	3171	1.5	1179
Conness Basin	CB-5	Metasediment	37.9928	119.2870	3140	1.3	1152
Ebbetts Pass	EP-24	Andesite	38.5655	119.8084	2530	4.8	1343
Ebbetts Pass	EP-25	Andesite	38.5665	119.8114	2549	4.8	1343
Ebbetts Pass	EP-26	Basalt	38.5473	119.8136	2732	3.9	1455
Ebbetts Pass	EP-28	Basalt	38.5483	119.8144	2744	3.9	1455
Mount Tallac	MT-38	Granodiorite	38.9430	120.1235	2134	6.5	1481
Mount Tallac	MT-39	Granodiorite	38.9420	120.1247	2195	6.5	1481
Grizzly Peak	GP-1	Basalt	37.8903	122.2346	393	13.8	727
Twin Peaks	TP-1	Pillow basalt	37.7504	122.4483	260	13.6	705
Twin Peaks	TP-2	Pillow basalt	37.7502	122.4476	252	13.6	705
Twin Peaks	TP-3	Chert	37.7533	122.4480	280	13.6	705
Twin Peaks	TP-4	Chert	37.7533	122.4480	280	13.6	705

[1]Mean annual temperature (Prism Climate Group, 2019)

[2]Mean annual precipitation (Prism Climate Group, 2019)

Table 2. Results

Pair	Fracture spacing[1] (mm)	a-axis diameter[1] (mm)	b-axis diameter[1] (mm)	c-axis diameter[1] (mm)	Fracture geometric stdev	b-axis geometric stdev	Erosion rate (mm/yr)	T_p (yrs)	Layers removed[3]
CB-1	330	375	250	130	0.346	0.357	0.02	125,000	0.8
CB-2	200	500	270	205	0.458	0.612	0.09	3,000	5.9
CB-3	280	720	420	190	0.551	0.477	0.05	8,400	2.3
CB-5	120	335	220	95	0.309	0.306	0.25	880	27
EP-24	80	225	150	55	0.283	0.255	0.31	484	50
EP-25	155	320	200	70	0.401	0.294	0.12	1,667	10
EP-26	60	95	55	25	0.285	0.201	0.68	81	150
EP-28	70	160	100	65	0.358	0.338	0.26	385	48
MT-38	390	1010	575	310	0.387	0.333	0.09	6,389	3.0
MT-39	200	850	570	280	0.411	0.352	0.14	4,071	9.1
GP-1	77	130	82	48	0.286	0.203	-	-	-
TP-1	10	-	10	-	0.251	0.328	-	-	-
TP-2	10	-	14	-	0.314	0.215	-	-	-
TP-3	24	-	27	-	0.214	0.14	-	-	-
TP-4	19	-	26	-	0.257	0.184	-	-	-

[1]Fracture spacings and particle diameters are reported as medians of distributions measured in field
[2]Cliff retreat rates were measured by Moore et al. (2009).
[3]Layers removed is the number of layers of thickness equal to the median fracture spacing that have been removed since the glacier retreated and is calculated as $13,000/T_P$, where T_P is calculated according to equation 1.
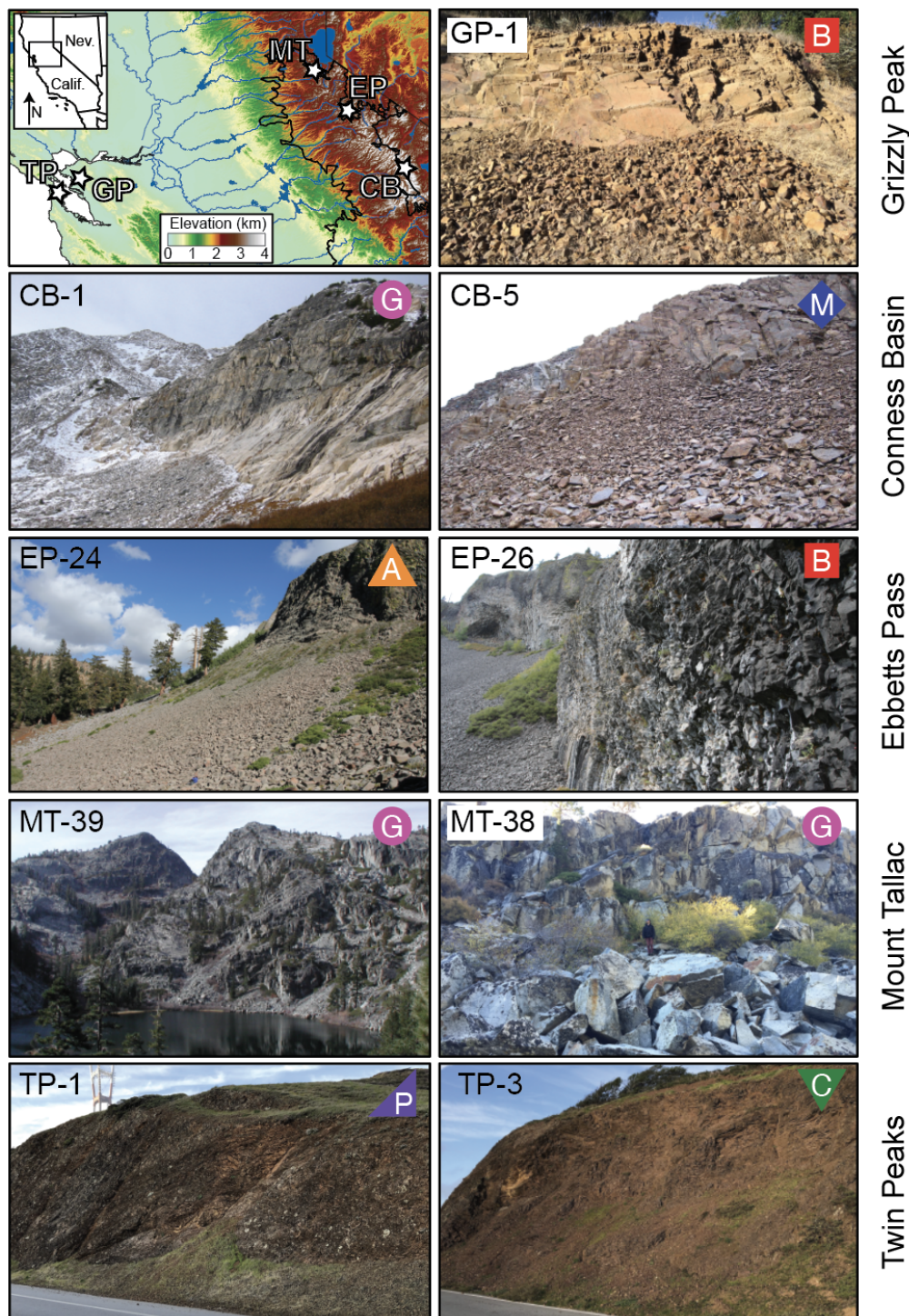
Figure 1. Study site map (upper left) and representative talus-cliff pairs from each site, with label designating lithology (red B squares = basalt; pink G circles = granodiorite; purple M diamond = metasediment; orange A triangles = andesite; purple P triangles = pillow basalt; green C triangles = chert). Scale varies between images. See Table 1 and text for site descriptions.
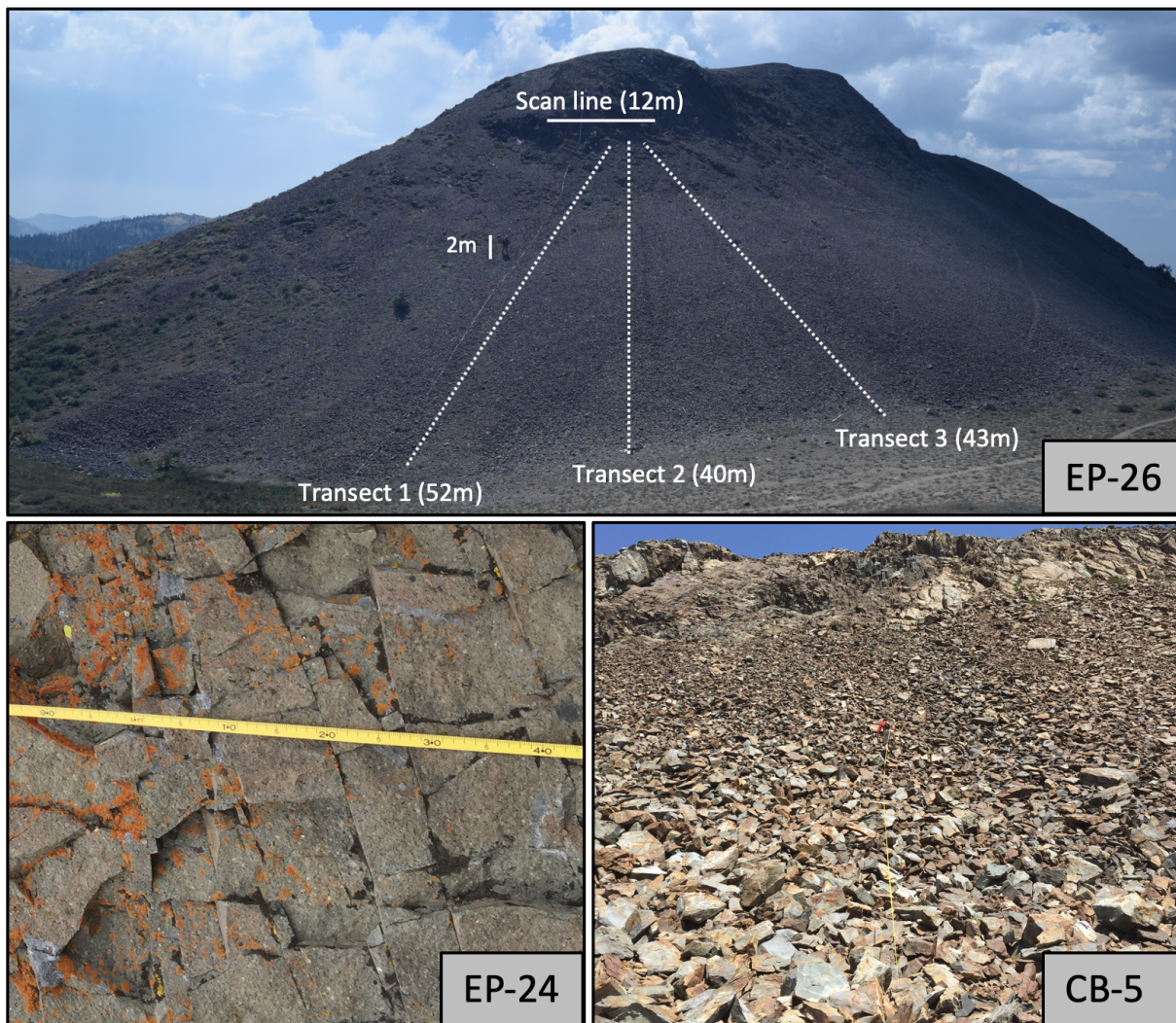
Figure 2. Field survey methods, showing example of transect line and scan line layout at EP-26 site in the Sierra Nevada (top) with detail of scan line at EP24 (lower left) and Transect 2 at CB-5 (lower right). Scale in the top image highlights a person near Transect 3. Tape in lower left is labeled in 10 cm increments.

Earth **Surface**
Dynamics
Discussions

EGU
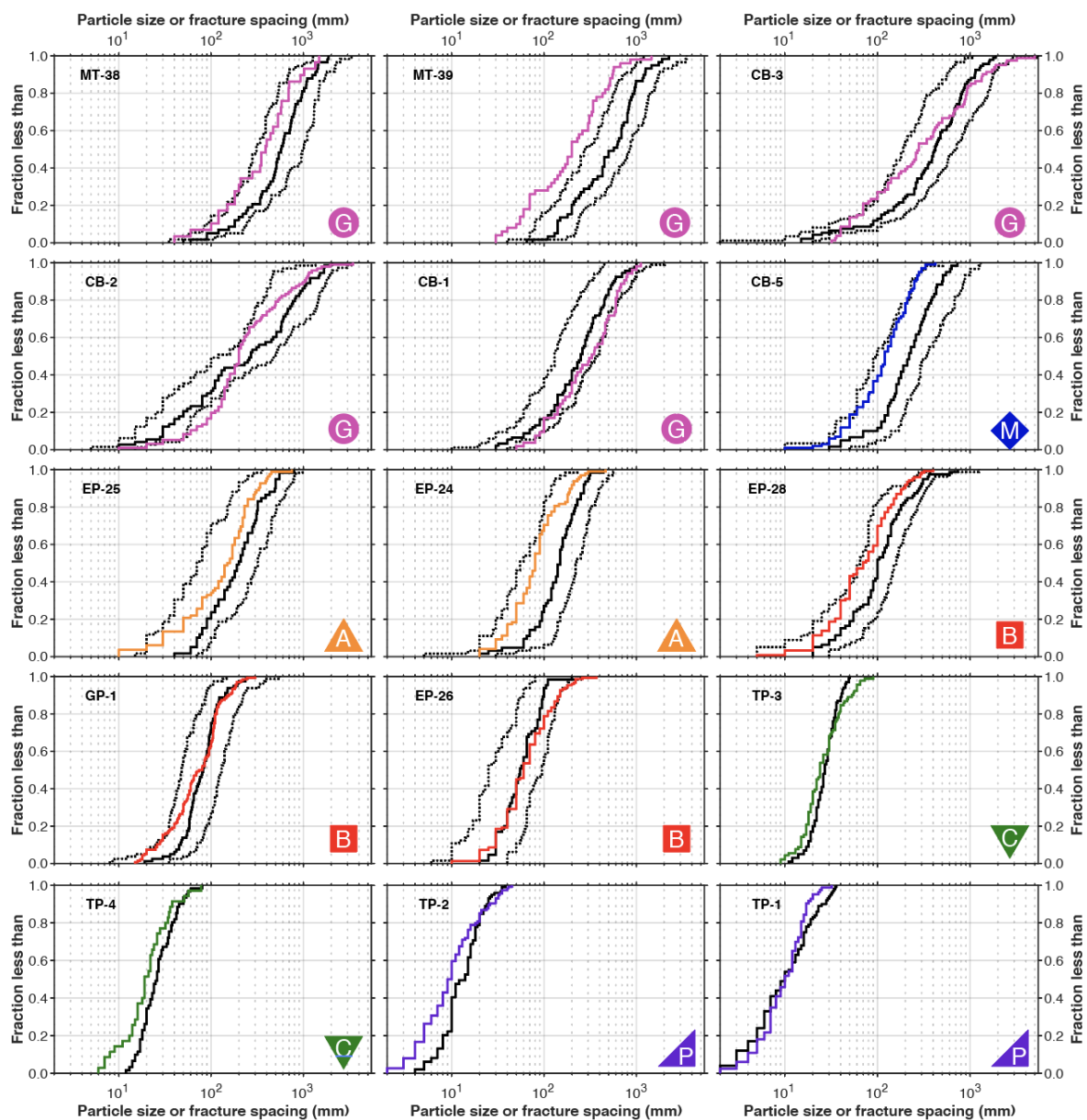
495

Figure 3. Particle size and fracture spacing distributions for each study site, sorted by median b-axis diameter in descending order from left to right and top to bottom. Colored lines show fracture spacing distributions, solid black lines show b-axis diameter distributions, dashed lines show a- and c-axis diameter distributions. (Major-axis diameters plot to the left of the intermediate-axis diameters). Color codes and labels for lithology are as in Fig. 1; see Table 1 for site abbreviations. At the

500   chert and pillow basalt sites, only b-axis diameters were measured (see text).
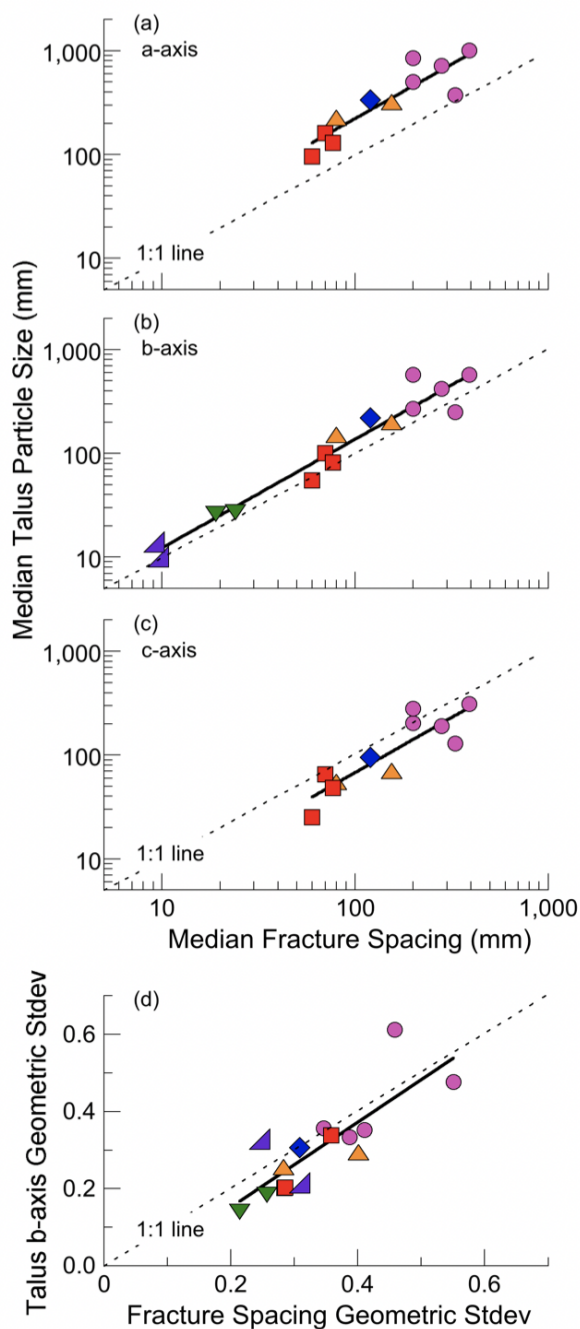
Figure 4. Central tendency and spread of particle size and fracture spacing distributions for median a-axis diameter (a), median b-axis diameter (b), median c-axis diameter (c), and the geometric standard deviation of the b-axis diameters (d). In each case, across the wide range in particle sizes and fracture spacings represented by the different lithologies sampled here, there are strong correlations between the particle size and the fracture spacing distributions that are roughly parallel with a 1:1 relationship (a–d). The correspondence is especially close for the b-axis diameters (b), though they are systematically 42% larger on average than the fracture spacings. Symbol type and color represent lithology as in Fig. 1.

Earth **Surface**
Dynamics
Discussions

EGU
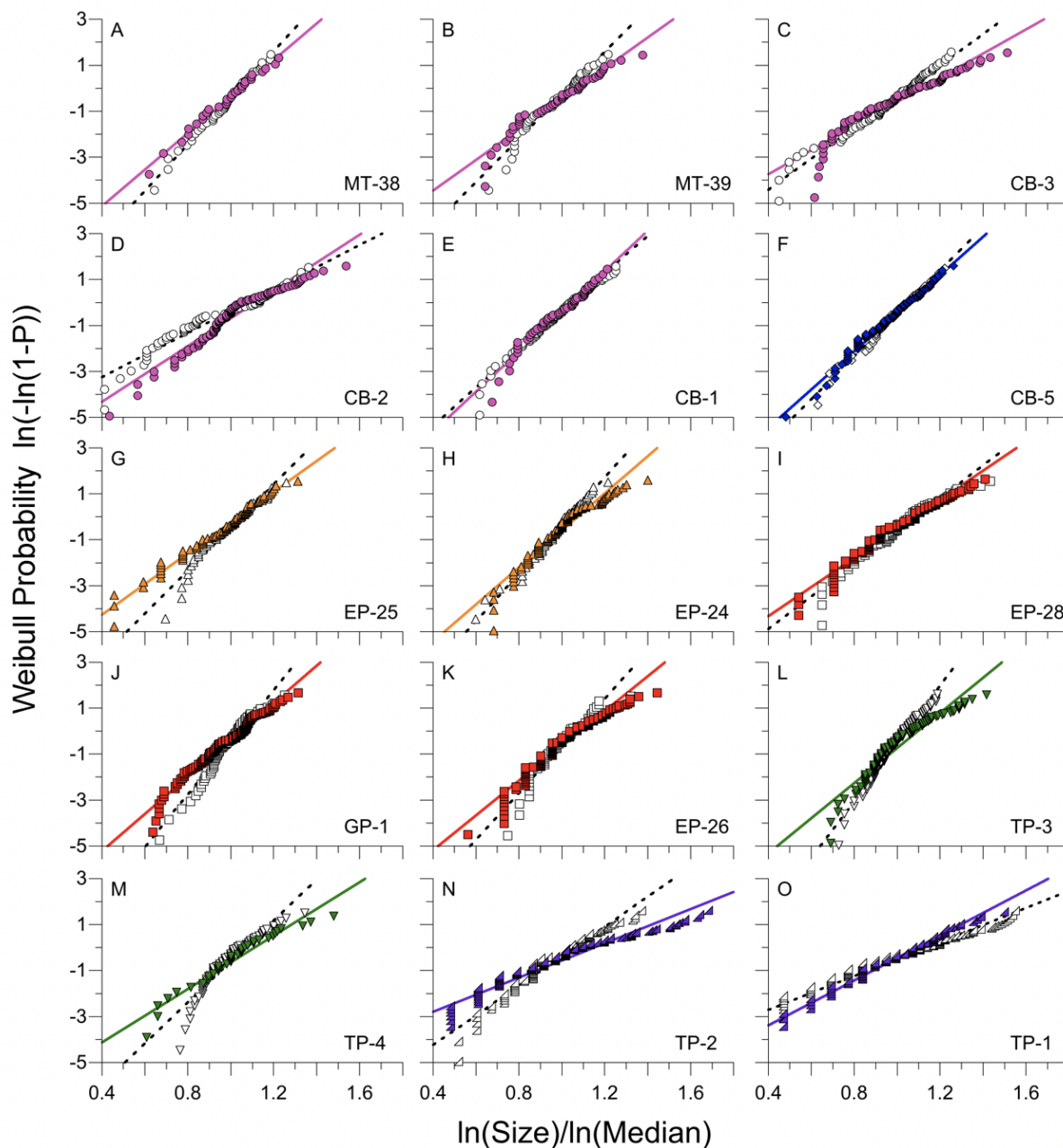
Figure 5. Comparison of distribution shape for the b-axis diameter (open symbols) and fracture spacing (colored) distributions in Weibull probability space. Points fall along a straight line in these plots when the sample is drawn from a population having a Weibull distribution. Best fit linear regressions for b-axis diameters and fracture spacings are shown as dashed and colored lines, respectively. Colors correspond to lithologies following conventions in Fig. 1. For most sites, most points plot along a straight line, implying that their population distributions are Wiebull-like. In addition, the data commonly overlap, consistent with a close match between the shape of the particle size and fracture spacing distributions at many of the sites. Examples and exceptions are highlighted in the text.

Earth **Surface**
Dynamics
Discussions
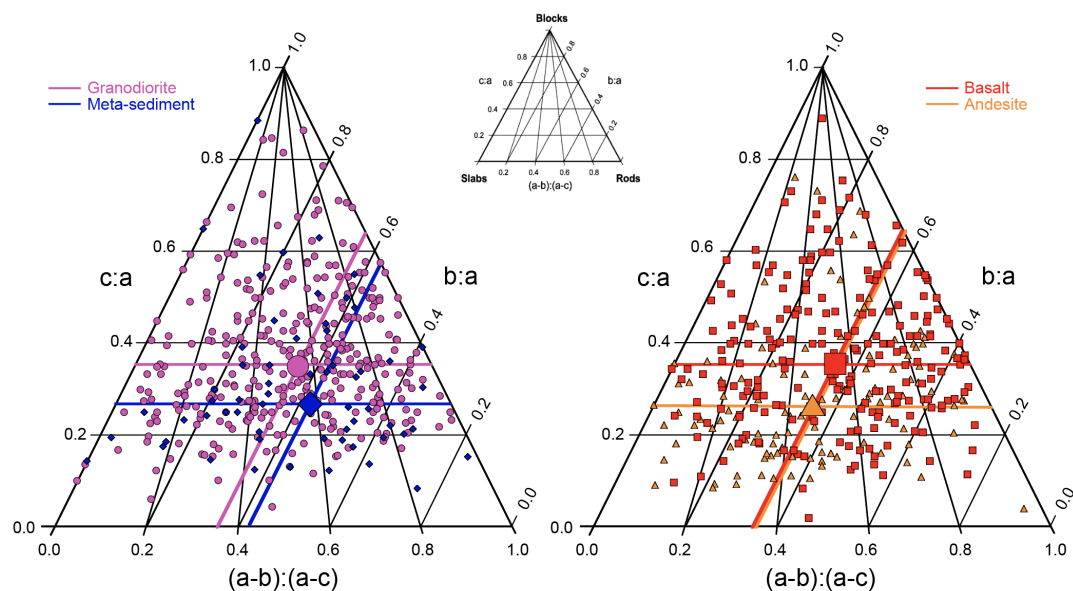
Figure 6. Particle shape at sites where all three particle diameters were measured as revealed in ternary diagrams with blocks, rods, and slabs at vertices (inset). Although data within each site and within each lithology are widely scattered in shape, the central tendencies for samples grouped by lithology yield several statistically significant differences. For example, granodiorite has a higher b:a and c:a ratio than the metasediment (left), indicating that metasediment is more rod-like on average. Symbols and colors represent lithology following conventions of Fig. 1.

520

Earth **Surface**
Dynamics
Discussions
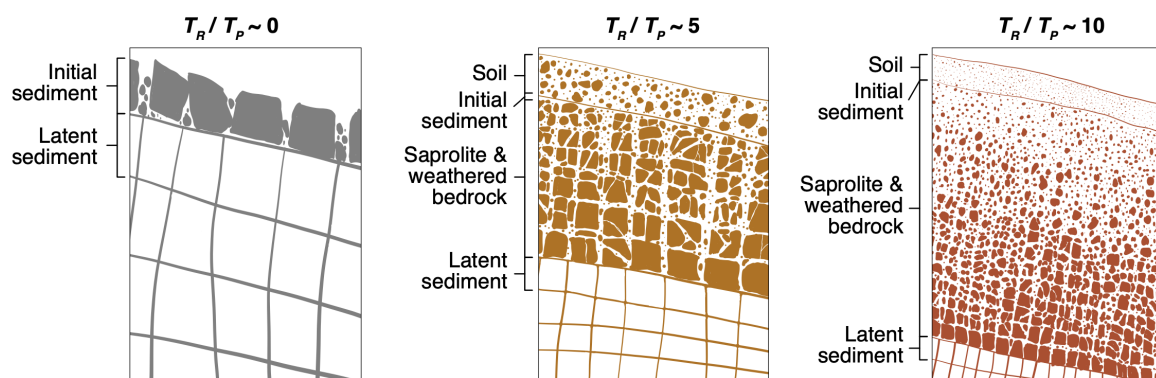
525 **Figure 7.** Conceptual framework illustrating how initial sediment size is influenced by latent sediment size and weathering. Panels depict vertical profiles of subsurface weathering where initial sediment is produced by detachment at the top of intact bedrock (a) or saprolite (b,c). Erosion rate is the same in each panel. Where fracture spacing is wide and where the weathering zone is thin, latent size should dominate over weathering (a), and vice versa where fractures are closely spaced and the weathering zone is comparatively thick (c). These examples lie on a spectrum of outcomes that correlate with the
530 ratio of two characteristic timescales: the timescale of weathering (T_R) and the time required to detach a layer of characteristic (median) particles at the base of mobile regolith (T_P). Higher ratios correspond to a greater influence of weathering and a lesser influence of latent size on initial sediment size distributions.